Fabrication and Microwave Characterization of 3D Printed Transmission Lines

Paul I. Deffenbaugh, Thomas M. Weller, Kenneth H. Church

***Abstract* — 3D printing has the potential to enable next generation manufacturing of RF and microwave circuits but little work has been done to demonstrate the true potential of this approach. This study shows that transmission lines fabricated using 3D printing equipment are comparable in performance to similar transmission lines fabricated using traditional methods, but opening the door to extreme design flexibility. Basic transmission line parameters such as characteristic impedance, effective dielectric constant, dielectric loss, and conductor loss are modeled and measured for a variety of materials and types of transmission lines at frequencies up to 10 GHz. Data is given for use in future 3D printed RF designs.**

***Index Terms*—3D printing, direct-digital manufacturing, microstrip, printed electronics, transmission line**

I. Introduction

3D printing has garnered immense attention from many fields including in-office rapid prototyping of mechanical parts, outer-space satellite replication [1], garage functional firearm manufacture [2], and NASA rocket engine component fabrication [3]. State of the art 3D printing is not only capable of fabricating structurally functional parts but due to improvements in accuracy it can also be used to rapidly manufacture 3D RF/microwave components [4]–[6]. The core advantages of 3D printing RF/microwave components include rapid prototyping of complex, dimensionally sensitive circuits (such as antennas and filters which are often iteratively tuned) and the ability to create new devices that cannot be made using standard fabrication techniques [4]. High frequency characterization at several levels is important. Measurement of the raw materials involved and microwave circuit analysis are important to capture the real-world performance of high frequency analog and digital signals. Recently, it has been demonstrated that the loss tangent of printed materials is acceptable for their incorporation in RF/microwave designs [6]. In general, fused deposition modeling (FDM) can utilize materials with low microwave loss but produces poor print resolution and a rough surface finish, while stereolithography (SL) exhibits excellent resolution and a smooth surface finish but the materials have more loss [6]. No work has been done to date which uses thick film silver paste or 3D printed SL material in a microwave application without copper plating. Also demonstrated here for the first time is a process of depositing thick film silver paste in printed ABS material in one machine.

This study models and measures the performance of SL and FDM substrate materials and a conductive thick film paste at DC and microwave frequencies in t-line structures. The SL resin ProtoTherm is seen to have a loss tangent of 0.03 and the FDM thermoplastic ABS is seen to have a loss tangent of 0.007. DuPont CB028 conductive paste is seen to have a DC resistivity of 21 μΩ•cm and an effective RF resistivity of 40 to 500 μΩ•cm depending on the type of t-line. Although these values are higher than high performance microwave circuit materials, 3D printing brings extreme flexibility in design and circuit layout which cannot be realized in a planar stack-up and it is these advantages which should attract microwave designers to 3D printing.

II. Fabrication

Seven different samples are fabricated, a non-printed microstrip, four microstrips, a stripline, and a suspended microstrip (Fig. 1-4). CB028 squares are printed to measure DC resistivity and ABS squares are printed to measure dielectric properties.

A. Stereolithography

SL parts (figures 1, 2, 7, 8) are fabricated using a 3D Systems Viper si2 with a layer thickness of 50.8 μm and 76.2 μm laser beam. Samples are printed on polycarbonate in order to eliminate support marks and preserve a smooth bottom surface. The ProtoTherm 12120 microstrip is 50 x 30 x 0.8 mm and has T_g = 111 °C increasing reducing CB028 conductivity. The suspended microstrip is 50 x 10 x 1.6 mm includes a 1 mm air gap suspending the conductor on 300 μm dia. pillars and WaterShed maximizes resolution (T_g = 41 °C).

B. Full 3D Printing

The nScrypt SmartPump precisely lays down screen-printable thick film silver paste in a mask-less, screen-less, arbitrary and rapidly reconfigurable fashion. The thermoplastic pump works similarly and allows printing of molten

Manuscript received April 1, 2014. Support by army contract # W911NF-13-1-0109, US ARMY RDECOM ACQ CTR - W911NF, Title: HBCU/MI: 3D Formable RF Mat. & Dev. Also: the TX Governor, Rick Perry under the TX Emerging Tech. Fund. Also: DARPA Contract # D14PC00016, Title: 3D Printed Wire Harness & Connectors for Satlets. The views expressed are those of the author(s) and do not reflect the official policy or position of the Department of Defense or the U.S. Government. Distribution Statement "A" (Approved for Public Release, Distribution Unlimited). Paul I. Deffenbaugh works in the W.M. Keck Center for 3D Innovation at UTEP in El Paso, Texas, 79902 USA (email: pdeffenbaugh@miners.utep.edu). Dr. Thomas M. Weller is with the Center for Wireless and Microwave Information Systems at the University of South Florida, Tampa, Florida, 33620, USA (email: weller@usf.edu). Dr. Kenneth H. Church is a professor in the UTEP Keck Center and CEO of nScrypt, Inc., Orlando, Florida, 32826, USA (email: khchurch@utep.edu).

thermoplastic. Pump switching on an nScrypt 3Dn-600 allows each of the six layers is laid down one after the other thus forming the multi-material (CB028/ABS) part from the bottom up. Paste curing occurs automatically on the 90 °C heated build plate. The process of printing conductive paste and dielectric in one process is termed "full 3D printing" (figure 3).

ABS is printed in 100 µm layers and CB028 is printed in 40 µm layers; the stripline is 50 x 30 x 0.8 mm. A partial lattice ground demonstrates paste savings while maintaining performance.

C. Comparison Sample Preparation

Microstrip comparison samples are fabricated on 50 x 30 x 0.762 mm Rogers RT/Duroid 5870 laminate (figure 3). A sample is fabricated using traditional masking and etching techniques. A sample is prepared by etching off all of the copper cladding and printing thick film silver paste (figure 4). A sample of copper on 1.6 mm FR-4 is measured (not shown). GigaLane SMA launches are soldered or bonded using EPO-TEK H20e conductive epoxy.


Figure 1 CB028 on ProtoTherm

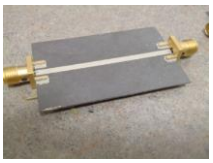
Figure 2 CB028 on Rogers

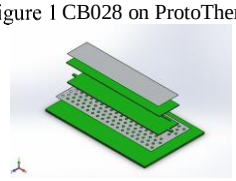
Figure 3 Stripline Layers

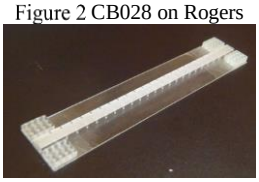
Figure 4 Suspended microstrip

III. Modeling

Ansys HFSS is used to model the SMA transition for the purpose of connector removal in the MATLAB analysis and to model the overall S-parameters of the microstrip lines. Extraction equations effectively remove the effects of the transitions from the measured data. Stripline samples are measured after SOLT probe calibration so no model calibration is required.

The Nicholson-Ross-Weir method [8] – [9] is used to obtain propagation coefficient (P) from measured S-parameters. The overall line loss (α_T) and effective permittivity (ε_e) are determined using (1) and (2). Overall loss is considered to follow (3). Nonlinear regression is used to determine the coefficients A and B in order to separate the dielectric loss (α_d) and conductor loss (α_c) which lead to loss tangent and resistivity [10] or [11].

$$\gamma = -\frac{1}{l}(lnP + i[\angle P - 2\pi N]) \quad N \in \mathbb{N} \tag{1}$$

$$\gamma = \alpha_T + j\frac{2\pi f\sqrt{\varepsilon_e}}{c_0} \tag{2}$$

$$\alpha_T = \alpha_d + \alpha_c = Af + B\sqrt{f} \tag{3}$$

Errors are magnified when the electrical length of the line is a multiple of ½ wavelength [9] therefore errors are minimized by using linear interpolation when the phase of S_{21} is {0, 90, 180, 270} ± 30 °.

IV. Measurement

The resistivity of 8x8 mm samples of printed paste are measured using an Ecopia HMS-5000 Hall Effect Measurement and an AlphaStep Profilometer, Data sheet min and max values are included in figure 9 along with the value for copper tape. CB028 achieves close it its minimum value at a cure temperature of only 100 °C.

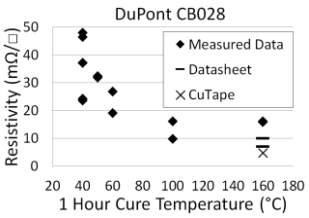

Figure 5 Conductor Properties

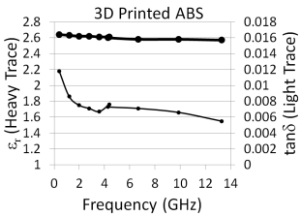

Figure 6 Dielectric Properties

The dielectric constant and loss tangent of the printed ABS is measured using a Damaskos 125HC (0.5 to 4.5 GHz) and a Damaskos 015 (4.5 GHz to 15 GHz) cavity. Figure 6 shows average values 2.6 and 0.007.

An HP 8720ES 20 GHz VNA obtains S-parameter data. Microstrip samples are measured using full two-port SOLT calibration performed using an Agilent 85033D 3.5 mm calibration kit. Picoprobes and a calibration wafer are used with the striplines. Figures 7-12 show the measured S-parameters (thick lines) and HFSS model data (thin lines).

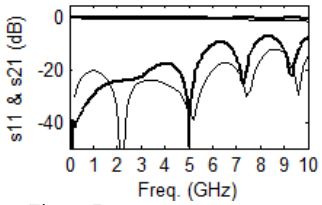

Figure 7 Cu on Rogers 5870 Microstrip

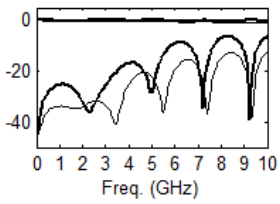

Figure 8 CB028 on Rogers 5870 Microstrip

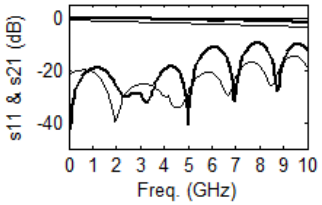

Figure 9 Cu on ProtoTherm Microstrip

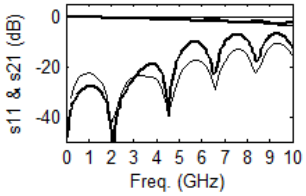

Figure 10 Fully 3D Printed Microstrip

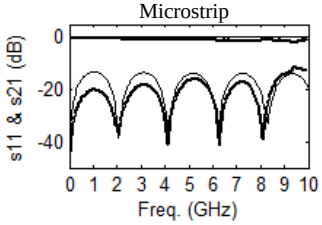

Figure 11 Fully 3D Printed Stripline

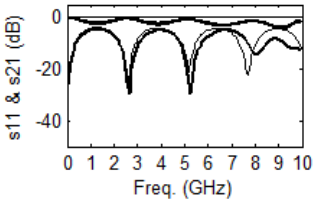

Figure 12 Fully 3D Printed Suspended Microstrip

S_{11} and S_{21} measured

S_{11} and S_{21} HFSS model

Parameter extractions for CB028 on ProtoTherm are shown

in figure 17. The properties of ProtoTherm are around $\varepsilon_r = 3$ and $\tan\delta = 0.03$ which match literature [7].

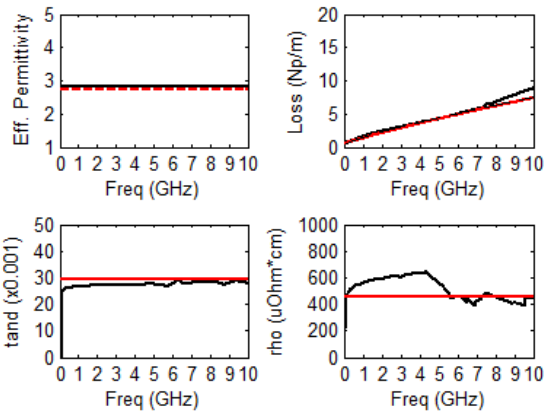

Legend: Measured, Least squares, Model

Figure 13 Fully 3D Printed Microstrip

Figure 14 shows the loss in each type of transmission line. Rojas has fabricated coplanar waveguide samples and the loss is reproduced here (black). Solid ProtoTherm microstrips (CB028: blue, Cu: blue-dash) have the highest loss due to the resin's loss tangent. The solid ABS stripline (green) comes in next due to the high loss of printable silver paste. The suspended microstrip (gray) is seen to have lower loss than the FR4 sample (red). The lowest loss lines are fabricated from Rogers 5870 (CB028: orange, Cu: orange -dash). Note that the absolute error in the measurement of the loss is worse with Rogers 5870 since the magnitude of the error is smaller.

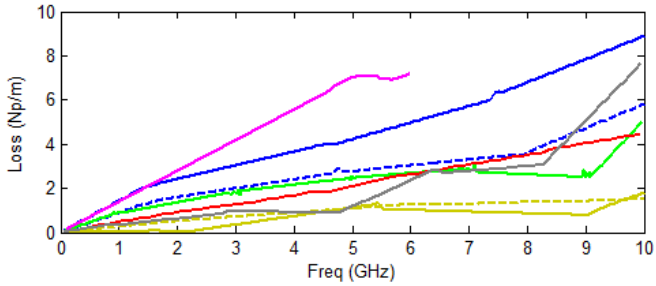

Figure 14 Loss Comparison by Material Stack-up, see text for legend

V. Conclusion

Table I shows a summary of the material and model data. The DC loss in CB028 is close to the data sheet specification of 7-10 mΩ/□/mil (about 22 μΩ•cm). CB028 paste works by deposition in a polymer carrier which is subsequently cured to drive off solvents and cause shrinkage and tightening of the flakes to form a highly conductive material. This process may affect the RF conductivity differently than if the material was a solid metal as in the case of copper.

The RF effective resistivity computed from S-parameters is 44 to 500 μΩ•cm depending on the type of transmission line. Each transmission line type has a different current transport profile across the cross-section. The RF characteristics of silver flake lines is not fully understood and further study is merited in this area. The insights gained will lead to better RF transmission lines in the future. Although the conductor loss mechanisms in 3D printable silver ink are not fully understood, the loss is accurately measured and it is now possible to design a transmission line with predictable loss using the information here. Based on the measurements which are performed, 3D printed materials are viable options for future RF and microwave devices. It is suggested that more elaborate RF/microwave components should be made which take advantage of the design flexibility, compactness, and rapidity of manufacture which 3D printing offers.

Table I
Design Guide for 3D Printed Stack-ups

Sample Type	$tan\delta$	ρ	α_d	α_c	α_T	α_T
CPW by Rojas	0.054	314.7	4.10	2.19	6.29	(7.04)
Cu/Rogers	0.0012	1.68	0.08	0.11	0.19	(0.36)
CB028/Rogers	0.0012	500	0.08	1.91	1.99	(1.08)
Cu/ProtoTherm	0.030	1.68	2.11	0.11	2.22	(2.76)
CB028/ProtoTherm	0.030	500	2.11	1.91	4.02	(4.22)
Stripline	0.012	44	1.25	1.40	2.66	(2.62)
FR-4	0.023	1.68	1.74	0.18	1.82	(2.15)
Suspend. Microstrip	0.030	100	0.51	0.51	1.03	(1.20)

Notes: Model/measurement-fitted data is given. Values in parenthesis are measured data. The data is given at 5 GHz. Units are μΩ·cm and Np/m.

References

[1] C. D. Gutierrez, "Three-dimensional structural electronic integration for small satellite fabrication," M.S. thesis, Elect. Eng., Univ. of Texas at El Paso, El Paso, TX, 2012, Available: http://digitalcommons.utep.edu/dissertations/AAI1512575.

[2] A. C. Estes. "Cody Wilson's Fully 3D-Printed Gun Works Alarmingly Well," Retrieved Dec. 5, 2013, Available: http://motherboard.vice.com/blog/cody-wilsons-fully-3d-printed-gun-works-alarmingly-well

[3] M. Gannon, "3D-Printed Rocket Part Passes Biggest NASA Test Yet," Retrieved Dec. 5, 2013. Available: http://www.space.com/22568-3d-printed-rocket-engine-test-video.html

[4] R.C. Rumpf and J. Pazos, "Synthesis of spatially variant lattices," Opt. Express, 15263-15274, 2012.

[5] K. Kirschenmann, et al., "Pastejet-printed microwave frequency multilayer antennas," IEEE Antennas and Propagation Society International Symposium, 2007, pp.924-927, June 9-15, 2007.

[6] Paul I. Deffenbaugh, Josh Goldfarb, Xudong Chen, Kenneth H. Church, "Fully 3D Printed 2.4 GHz Bluetooth/Wi-Fi Antenna," IMAPS, 46th International Symposium on Microelectronics, Orlando, Florida, September 30 – October 3, 2013

[7] P.I. Deffenbaugh, R.C. Rumpf, K.H. Church, "Broadband Microwave Frequency Characterization of 3-D Printed Materials," IEEE Transactions on Components, Packaging and Manufacturing Technology

[8] W. B. Weir, "Automatic measurement of complex dielectric constant and permeability at microwave frequencies," Proceedings of the IEEE, vol.62, no.1, pp.33-36, Jan. 1974.

[9] T. L. Blakney, W. B. Weir, "Comments on "Automatic measurement of complex dielectric constant and permeability at microwave frequencies," Proceedings of the IEEE, vol.63, no.1, pp. 203- 205, Jan. 1975.

[10] R. A. Pucel, et al., "Losses in Microstrip," IEEE Transactions on Microwave Theory and Techniques, vol.16, no.6, pp.342-350, June 1968.

[11] D. M. Pozar, "Microwave Engineering," 4th edition, Wiley, pp.147-149, 2012.

[12] P.I. Deffenbaugh, "3D Printed Electromag. Trans. and Electr. Structures Fabricated on a Single Platform using Advanced Process Integration Techniques," Ph.D. dissertation, Elect. & Comput. Eng., UTEP, El Paso, TX, 2014.

[13] E.A. Rojas-Nastrucci, T. Weller, V. Lopez Aida, F. Cai, J. Papapolymerou, "A Study on 3D-Printed Coplanar Waveguide with Meshed and Finite Ground Planes," WAMICON 2014, Jun. 2014.